Styrene-Based Poly(ethylene oxide) Side-Chain Block Copolymers as Solid Polymer Electrolytes for High-Voltage Lithium-Metal Batteries

Andreas J. Butzelaar,[#] Philipp Röring,[#] Tim P. Mach, Maxi Hoffmann, Fabian Jeschull, Manfred Wilhelm, Martin Winter, Gunther Brunklaus,[*] and Patrick Théato[*]

ABSTRACT: Herein, we report the design of styrene based poly(ethylene oxide) (PEO) side chain block copolymers featuring a microphase separation and their application as solid polymer electrolytes in high voltage lithium metal batteries. A straightforward synthesis was established, overcoming typical drawbacks of PEO block copolymers prepared by anionic polymerization or ester based PEO side chain copolymers. Both the PEO side chain length and the LiTFSI content were varied, and the underlying relationships were elucidated in view of polymer compositions with high ionic conductivity. Subsequently, a selected composition was subjected to further analyses, including phase separated morphology, providing not only excellent self standing films with intrinsic mechanical stability but also the ability to suppress lithium dendrite growth as well as good flexibility, wettability, and good contacts with the electrodes. Furthermore, good thermal and electrochemical stability was demonstrated. To do so, linear sweep and cyclic voltammetry, lithium plating/stripping tests, and galvanostatic overcharging using high voltage cathodes were conducted, demonstrating stable lithium metal interfaces and a high oxidative stability of around 4.75 V. Consequently, cycling of Li|NMC622 cells did not exhibit commonly observed rapid cell failure or voltage noise associated with PEO based electrolytes in Li|NMC622 cells, attributed to the high mechanical stability. A comprehensive view is provided, highlighting that the combination of PEO and high voltage cathodes is not impossible *per se*.

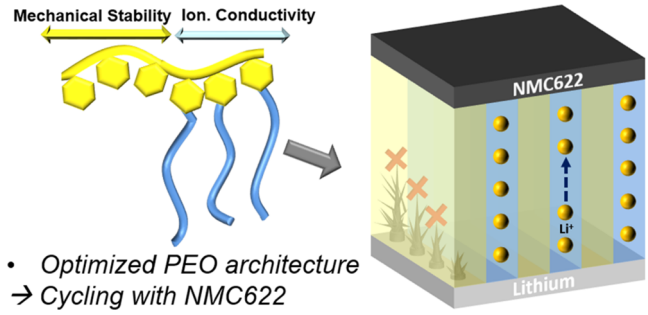

KEYWORDS: *solid polymer electrolyte, PEO architecture, microphase separation, high voltage cathode, NMC622, lithium metal battery, dendrite suppression*

1. INTRODUCTION

Fulfilling the growing requirements of batteries due to the rising market concerning, e.g., electric mobility, new active materials providing higher energy densities than the state of the art lithium ion batteries (LIBs) need to be commercialized,[1] for which higher specific capacities as well as higher anode/cathode potential differences need to be targeted.[2] In comparison to lithiated graphite, lithium metal offers high specific capacity and a lower redox potential, though its use is limited due to safety concerns in particular when paired with liquid electrolytes, originating from an instable solid electrolyte interphase (SEI) and lithium dendrite growth during cycling, leading eventually to short circuits.[3] To solve this problem, solid state electrolytes (SSEs) could provide sufficient mechanical strength to suppress lithium dendrite penetration.[4] In this regard, especially poly(ethylene oxide) (PEO) as part of solid polymer electrolytes (SPEs) is of high interest due to its good chain flexibility, low glass transition temperature (T_g), remarkable electrochemical stability against lithium metal, low comparable costs, and great solubility for conductive lithium salts.[5] Furthermore, PEO based SSEs are so far the only commercially used electrolytes in solid state batteries. The so called lithium metal polymer (LMP) battery was introduced by the Bolloré Group over the last decade, featureing a Li|PEO|$LiFePO_4$ (LFP) cell setup delivering 180 Wh kg^{-1} at temperatures between 60 and 80 °C, which is suitable for the automotive market, e.g., bluecar and bluebus.[6,7]

However, despite these important attributes and great achievements, PEO based SPEs often suffer from high crystallinity, which results in low ionic conductivities below its melting point due to the fact that ion transport is only taking place in the amorphous regions.[8,9] Therefore, to improve the ionic conductivity at lower temperatures, different approaches can be used to render the material completely amorphous, such as cross linking,[10] the implementation of

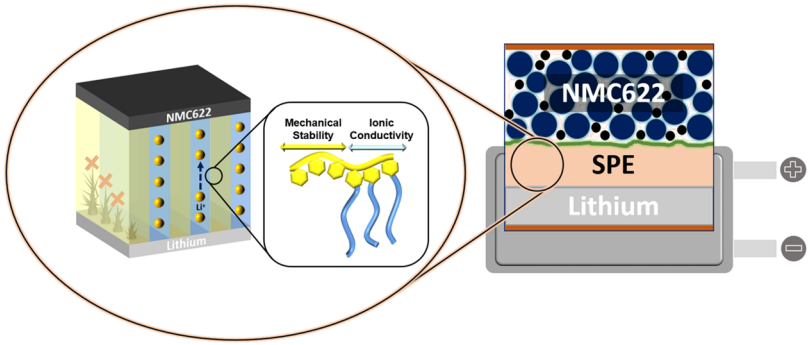

Figure 1. Schematics of dendrite suppression by microphase separation of block copolymers. As soon as a dendrite is in contact with the mechanically rigid block, its growth is stopped or significantly slowed down, depending on mechanical or local electric field effects.

plasticizers[11,12] or nanofillers,[13] or blending with other polymers.[14] Furthermore, approaches to alter the molecular architecture, such as side chain or cage architectures, are successfully reducing crystallization to a significant amount, as we and others could demonstrate.[15−17]

Though completely amorphous PEO results in a loss of dimensional stability at room temperature due to the low T_g at around −65 °C,[5,18] high molar mass or cross linked polymers are solving this problem, partially providing substantial chain entanglement and, therefore, a macroscopically stable material. However, the soft matrix characterized by the low T_g does not provide sufficient resistance against lithium dendrite pene tration. In addition, it was shown recently that lithium dendrite penetration and not insufficient oxidative stability might also be the reason why PEO based SPEs cannot be used in combination with high voltage cathode materials such as $Li[Ni_{0,6}Mn_{0,2}Co_{0,2}]O_2$ (NMC622).[19−22]

In this regard, for PEO based SPEs, a tradeoff is established where a low T_g provides better ionic conductivity but insufficient mechanical stability, whereas a high T_g affords better mechanical stability but at the expense of reduced ionic conductivity. To solve this problem, it is necessary to tune both properties independent of each other. For this purpose, block copolymers have demonstrated to be successful by achieving this goal through the introduction of one PEO based polar block, as well as a high T_g nonpolar block, such as poly(styrene) (PS).[23] From self assembly of these block copolymers, e.g., via slow solvent evaporation, phase separated polar and nonpolar microdomains are formed, where one domain (usually the polar PEO domain) contributes to the ion transport, whereas the other domain (usually nonpolar high T_g domain) provides mechanical stability, hence, when properly balanced, yielding macroscopically solid block copolymer films (Figure 1).[24,25] Most examples described in the literature focus on block copolymers, such as PS *b* PEO, that were prepared by anionic polymerization, which is both tedious and highly dangerous when ethylene oxide gas is utilized.[26−28] Other examples describe the synthesis of block copolymers derived from PS and commercially available oligo(ethylene glycol) methyl ether methacrylate (OEGMA).[29,30] However, the ester moieties of the methacrylate provide a chemical weak point in terms of thermal and electrochemical stability as well as against nucleophilic impurities.[30,31]

Herein, we describe a synthetic approach toward block copolymers that overcomes both of the before mentioned drawbacks by exploiting styrene monomers featuring a side chain PEO, resulting in block copolymers with a thermally and (electro)chemically stable backbone. In addition, PS was chosen for the nonconducting block to provide a good mechanical stability due to its T_g of around 100 °C,[32] affordable price, and exceptional compatibility regarding the polymerization because of the possibility of using straightfor ward, reversible addition−fragmentation chain transfer (RAFT) polymerization. Furthermore, the side chain approach reduces the inherent crystallinity, while the microphase separation of the block copolymers allows for the preparation of a macroscopically self standing, truly "dry" SPE having both good flexibility and intrinsic mechanical stability (Figure 1). Based on our previous study regarding PEO side chain architectures, we briefly examined the impact of different PEO side chain lengths as well as the LiTFSI content on the thermal properties as well as the ionic conductivity of the derived microphase separated SPEs. We selected the block copolymer composition providing the highest ionic con ductivity to proceed with further detailed thermal, mechanical, and electrochemical characterization, eventually illustrating successful long term cycling in lithium metal||NMC622 full cells.

2. EXPERIMENTAL SECTION

2.1. Materials. Sodium hydride (60% dispersion in mineral oil, Aldrich), poly(ethylene oxide) monomethyl ether (mPEOz, "*z*" = 400, 1000, 2000 equals to M_n = 400, 1000, 2000 g mol^{-1}, TCI), 4 vinylbenzyl chloride (90%, Aldrich), and 2 (dodecylthiocarbono thioylthio) 2 methylpropionic acid (98%, Aldrich) were used as received. Bis(trifluoromethane)sulfonimide lithium salt (LiTFSI, 99.95%, Aldrich) was dried at 80 °C under vacuum for 2 days and subsequently stored inside a glove box (MBraun Unilab, <0.1 ppm H_2O, <0.1 ppm O_2) under an inert argon atmosphere. Styrene (99%, Acros) was passed through basic alumina oxide prior to use. All other solvents and reagents were of analytical grade or higher and were used without further purification.

2.2. Macromonomer Synthesis (4-Vinylbenzyl mPEOz, VBmPEOz). Sodium hydride (60% dispersion in mineral oil, 1.5 equiv pure NaH, 0.075 mol L^{-1}) was placed in a round bottom flask with an appropriate amount of dry tetrahydrofuran (THF) and purged with dry N_2 for 15 min while stirring. Afterward, mPEOz (1.00 equiv, 0.05 mol L^{-1}) was added dropwise (solid mPEOz was dissolved in dry THF prior to addition) and the mixture was stirred until no more gas development was observed (between 15 and 30 min). Then, 4 vinylbenzyl chloride (3.00 equiv, 0.15 mol L^{-1}) was slowly added. The reaction mixture was stirred overnight. Afterward, the reaction was quenched with 10 mL of deionized water and concentrated under reduced pressure. Water and dichloromethane (DCM) were added to separate the phases. The organic phase was washed with water four times, and the aqueous phase was re extracted once with DCM. The combined organic phases were dried over $MgSO_4$, filtered, and the

solvent was concentrated under reduced pressure. Subsequently, the product was precipitated four times from THF into cold diethyl ether and centrifuged. The product was obtained as a slightly yellow liquid (z = 400) or as a slightly yellow/white solid (z = 1000/2000) and dried at 40 °C under vacuum overnight. Yields: 80−95%

2.2.1. ^{1}H NMR (400 MHz, CDCl$_3$). δ/ppm = 7.39−7.28 (m, 4H, $C_{Ar}\mathbf{H}$), 6.74−6.67 (dd, J = 17.6, 10.9 Hz, 1H, $H_2C{=}C\mathbf{H}$), 5.75−5.71 (d, J = 17.6 Hz, 1H, $\mathbf{H}_{cis}HC{=}CH$), 5.24−5.21 (d, J = 10.9 Hz, 1H, $\mathbf{H}_{trans}HC{=}CH$), 4.54 (s, 2H, $CC\mathbf{H}_2O$), 3.68−3.52 (m, xH, $OC\mathbf{H}_2C\mathbf{H}_2$), 3.37 (s, 3H, $OC\mathbf{H}_3$).

Integrals: z = 400: x = 38, z = 1000: x = 101, z = 2000: x = 194.

2.2.2. ^{13}C NMR (400 MHz, CDCl$_3$). δ/ppm = 138.01 (s, 1C, $CH\mathbf{C}_{tert.}CH$), 137.04 (s, 1C, $CH_2\mathbf{C}_{tert.}CH$), 136.69 (s, 1C, $H_2C{=}\mathbf{C}H$ $C_{tert.}$), 128.03 (s, 2C, $CH_2C_{tert.}\mathbf{C}H$), 126.30 (s, 2C, CH $C_{tert.}\mathbf{C}H$), 113.82 (s, 1C, $H_2\mathbf{C}{=}CH$), 73.04 (s, 1C, $C_{tert.}\mathbf{C}H_2O$), 72.04 (s, 1C, $\mathbf{C}H_2OCH_3$), 70.74 (m, $[OC\mathbf{H}_2\mathbf{C}H_2]_n$), 69.49 (s, 1C, $C_{tert.}CH_2O\mathbf{C}H_2CH_2$), 59.12 (s, 1C, $\mathbf{C}H_3$).

2.3. Homopolymerization of VBmPEOz. 2 (Dodecylthiocarbonothioylthio) 2 methylpropionic acid (DDMAT, 1.00 equiv) was dissolved in a 1:1 mixture of water and dioxane in a round bottom flask. VBmPEOz (z = 400: 30.0 equiv, 0.65 mol L^{-1}, z = 1000: 15.0 equiv, 0.45 mol L^{-1}, z = 2000: 9.00 equiv, 0.35 mol L^{-1}) and 2,2′ azobis(2 methylpropionitrile) (0.50 equiv) were added subsequently. The solution was purged with N_2 for 20 min, and the polymerization was conducted at 80 °C for 23 h. Subsequently, the polymerization was stopped by placing the flask in the freezer. Then, the solvent was removed under reduced pressure. Poly(VBmPEO400) was obtained as a highly viscous, yellow liquid and poly(VBmPEO1000) and poly(VBmPEO2000) were obtained as a solid product and used directly as macro RAFT agents for the block copolymerization. Yields: 100%

2.4. Block Copolymerization. The previously obtained macro RAFT agent (**poly(VBmPEOz)**, 1.00 equiv, z = 400: 0.014 mol L^{-1}, z = 1000: 0.013 mol L^{-1}, z = 2000: 0.009 mol L^{-1}) was dissolved in dioxane and styrene (z = 400: 200 equiv, 2.88 mol L^{-1}, z = 1000: 200 equiv, 2.54 mol L^{-1}, z = 2000: 500 equiv 4.37 mol L^{-1}) as well as AIBN (0.5 equiv) were added. The reaction was purged with N_2 for 10 min and polymerized at 80 °C for 23 h. Subsequently, the product was precipitated into diethyl ether, redissolved in THF, and reprecipitated in diethyl ether three times. The resulting polymer was dried at 50 °C under vacuum overnight. Yields: 80−90%

2.5. Solid Polymer Electrolyte (SPE) Preparation. Prior to the SPE membrane preparation, the respective polymer was dried at 80 °C under vacuum (10^{-3} mbar) overnight. The polymer as well as the corresponding amount of LiTFSI with predefined ratios of [Li$^+$]/[EO] 1:5, 1:10, 1:15, or 1:20 were dissolved in acetonitrile (MeCN). Subsequently, the solution was poured into a Teflon mold. The mold was covered and MeCN was allowed to evaporate slowly at ambient conditions, enabling microphase separation. Subsequently, the obtained SPE film was dried and simultaneously annealed at 120 °C under vacuum (10^{-3} mbar) for 24 h. The film thickness for all measurements was around 100 μm.

2.6. Cathode Preparation. For the preparation of the cathodes, 0.9 g of NMC622 (BASF Toda, 90 wt %) or 0.9 g of Li[$Ni_{0.5}Mn_{1.5}O_4$] (LNMO) (kindly provided by Binder,[33] 90 wt %), 0.07 g of conductive carbon (Super P, Imerys, 7 wt %), and 0.03 g of binder (poly(vinylidene fluoride) (PVdF) 1100, Kureha, 3 wt %) were weighed in a sample container and 2 mL of *N* methyl 2 pyrrolidone (NMP) was added. The container was transferred to a Thinky centrifugal mixer and stirred twice for 5 min at 1700 rounds per minute. Then, the resulting homogeneous slurry was cast onto an aluminum current collector using a doctor blade technique with a gap width of 50 μm. The coating was dried in an oven at 80 °C overnight. To obtain a homogeneous thickness and surface, the cathode sheets were roll pressed to a final thickness of ∼40 μm (20 μm aluminum current collector, 20 μm electrode coating), resulting in a mass loading of ∼1.8 mg cm^{-2}. Round disks with a diameter of Ø = 12 mm were punched out and dried at 120 °C under vacuum (10^{-3} mbar) prior to use.

2.7. Electrochemical Impedance Spectroscopy (EIS). Ionic conductivities of polymer electrolyte films were measured by electrochemical impedance spectroscopy (EIS). The samples were prepared by placing the polymer electrolyte film between two stainless steel electrodes (2 setups with cells of 8 mm and 10 mm diameter) in a Swagelok type cell setup. All samples were preconditioned overnight, in a temperature chamber (TestEquity model 115A) at 65 °C, to improve the interfacial contact between the electrodes and electrolytes. The measurements were carried out using a VSP, SP 200, and SP 300 potentiostat (BioLogic Science Instruments) in a temperature range between 5 and 85 °C. An impedance measurement was conducted over a frequency range from 1 MHz to 500 mHz (and reverse) with an amplitude of 20 mV. A heating cycle comprised of a gradual temperature increase in 10 °C steps from 5 to 85 °C. The temperature was increased with a heating/cooling rate of 60 °C h^{-1} over 10 min, after which the temperature was held constant for another 50 min to acquire impedance spectra. At a temperature of 85 °C, the heating profile was reversed and gradually cooled down to 5 °C in similar temperature steps. The ionic conductivity σ was calculated according to eq 1.

$$\sigma = \frac{1}{R_b} \cdot \frac{l}{A} \tag{1}$$

R_b is the bulk electrolyte resistance that can be accessed from the Nyquist plot, l is the film thickness, and A is the film area.

2.8. Measurement of the Transference Number. The measurement of the transference number was performed on a VMP3 potentiostat (BioLogic Science Instruments) at 60 °C. For the measurements, symmetrical Li|SPE|Li cells were assembled. After the cells were conditioned for 1 h, impedance measurements were conducted every 4 h for a total of 20 h to guarantee a stable interface between the SPE and lithium metal (Honjo Metal, thickness of 300 μm). Impedance data were collected between a frequency of 1 MHz and 100 mHz with an amplitude of 10 mV. Direct current polarization was applied with a polarization voltage of ΔV = 10 mV, while the impedance was measured directly before and after the polarization, respectively. The data were evaluated using an equivalent circuit model, as depicted in Figure 4a, consisting of one resistor mirroring the electrolyte resistance, two RC elements reflecting the charge transfer as well as the SEI, and the Warburg element showing diffusion processes from/to the electrodes. The transference number t_{Li+} was calculated using eq 2, where I_s is the steady state current, ΔV is the polarization voltage, and R_0 and R_s are the electrode resistance (R_{CT} and R_{SEI}) before and after the polarization, respectively.

$$t_{Li^+} = \frac{I_s(\Delta V - I_0 R_0)}{I_0(\Delta V - I_s R_s)} \tag{2}$$

$$I_0 = \frac{\Delta V}{R_b + R_0} \tag{3}$$

The initial current I_0 is calculated using eq 3. R_b is the resistance of the polymer electrolyte and is determined by the impedance spectrum before polarization. Note that the initial current I_0, which is calculated by eq 3, is equal to the experimental value, which can be derived from the polarization plot.

2.9. Potentiodynamic Experiments. The electrochemical stability of the polymer electrolyte was measured in a Swagelok type three electrode setup by conducting linear sweep voltammetry (LSV) and cyclic voltammetry (CV) on a VSP potentiostat (BioLogic Science Instruments) at room temperature. Lithium was used as counter and reference electrodes and copper or platinum as the working electrode for the measurement of reductive or oxidative stability, respectively. LSV was conducted within a potential range of −0.5 and 7.0 V vs Li|Li$^+$ and a sweep rate of 0.1 mV s^{-1}. For CV measurements, three cycles were measured on copper as a working electrode between a potential range of −1.0 and 3.0 V vs Li|Li$^+$ and a scan rate of 0.1 mV s^{-1}.

For the measurement of limiting current density, LSV was conducted in symmetrical Li|SPE|Li coin cells with a sweep rate of

Scheme 1. Sequential Block Copolymerization by (a) Polymerizing VBmPEOz Obtaining a So Called Macro RAFT Agent (PVBmPEOz), Followed by (b) Chain Extension with Styrene Eventually Yielding PVBmPEOz *b* PS (BPz)

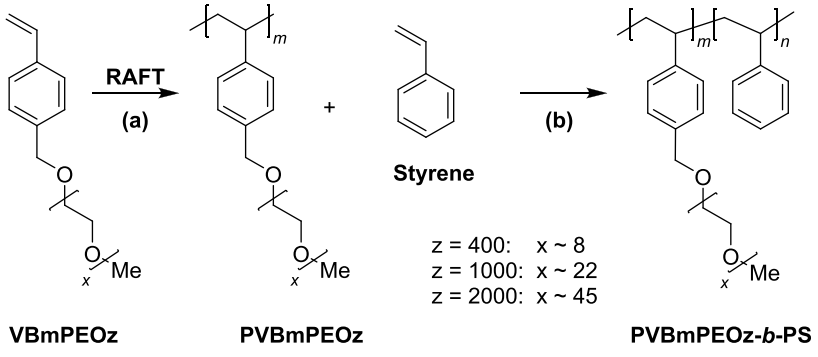

0.02 mV s^{-1} until a cut off voltage of 0.35 V vs LilLi$^+$. The reached plateau indicates the limiting current density.

2.10. Constant Current Cycling Experiments. All constant current cycling experiments were performed in a coin cell type two electrode setup using a Maccor series 4000 battery cell test system. The cells were conditioned at 60 °C in a climate chamber (Binder KB 400). Lithium plating and stripping experiments were performed in a symmetrical lithium cell. Prior to long term plating/stripping, the cells were conditioned with a current density of 0.05 mA cm^{-2} for 10 cycles. Afterward, lithium was constantly plated and stripped with a current density of 0.1 mA cm^{-2} for 1 h over 500 cycles (1000 h) or for 4 h over 37 cycles (296 h), respectively.

For the plating and stripping experiments with alternating current densities, 30 cycles with a current density of 0.1 mA cm^{-2} were conducted before the current density was increased stepwise for 10 cycles, each with 10 cycles at 0.1 mA cm^{-2} in between until a short circuit was observed or the safety limits were reached.

Galvanostatic overcharging was conducted (upper voltage limit of 6 V) with a specific current of 14.7 or 18.0 mA g^{-1} (~0.1C) for LNMO or NMC622 cathodes, respectively. The discovered voltage plateau was taken as an indication for the onset of the oxidative decomposition of the polymer electrolyte against cathode active materials.

Full cell cycling experiments were performed between 3.0 and 4.3 V vs LilLi$^+$ at a C rate of 0.1C. For rate performance experiments, alternating charge rates were used, whereas the discharge rate was maintained at 0.1C. Three cycles at 0.05C were conducted as formation prior to cycling.

The corresponding impedance data of the symmetrical lithium cells or full cells were collected using an Autolab PGSTAT204 potentiostat in a frequency range of 1 MHz−10 mHz with an amplitude of 10 mV. The EIS measurements were performed at a cell voltage of 0 V for symmetrical lithium cells and in a discharged state (3 V) for full cells. Data were collected before and after the formation and after the cycling of the corresponding cells.

2.11. Nuclear Magnetic Resonance (NMR) Spectroscopy. ^{1}H NMR (400 MHz) and ^{13}C NMR (101 MHz) spectra were recorded on a Bruker Ascend 400 NMR spectrometer at ambient temperature using chloroform d_1 as a deuterated solvent.

2.12. Thermal Gravimetric Analysis (TGA). Thermal gravi metric analysis (TGA) was carried out using a TGA 5500 (TA Instruments) at a heating rate of 10 K min^{-1} under a nitrogen atmosphere up to 800 °C.

2.13. Differential Scanning Calorimetry (DSC). Differential scanning calorimetry was conducted using a DSC Q200 (TA Instruments) ranging from −75 to 130 °C with a scan rate of 5 K min^{-1} for all measurements.

2.14. Size Exclusion Chromatography (SEC). Size exclusion chromatography was carried out in THF on a Tosoh Bioscience HLC 8320GPC EcoSEC system equipped with 3 PSS SDV columns, 5 μm (100, 1000, 100 000 Å) (8 × 300 mm^2), and a UV and a differential refractive index (RI) detector. The operation temperature was set to 35 °C with a flow rate of 1 mL min^{-1}. The system was calibrated using poly(styrene) standards ranging from 800 to 2.2 × 10^6 g mol^{-1}. Typically, 50 μL of a 2.0 mg mL^{-1} sample solution was injected onto the columns.

2.15. Small-Angle X-Ray Scattering (SAXS). The morphology of the block copolymers was investigated by two dimensional (2D) SAXS measurements on a Hecus S3 Micro X ray system using a point microfocus source, 2DX ray mirrors, and a two dimensional CCD detector from Photonic Science. Low background scatter was ensured by the use of a block collimation system. Samples were taken from the films obtained by the SPE preparation. 2D Spectra were radial averaged using self developed plugins for ImageJ, corrected for absorption and primary beam intensity. Normalization of the q range was done using crystalline silver behenate as a standard.

2.16. Oscillatory Rheology. Rheological measurements were performed on a strain controlled ARES G2 (TA Instruments) rheometer via small amplitude oscillatory shear experiments. The samples were prepared from the films obtained by the SPE preparation with 8 mm in diameter and 0.5 mm in thickness.

3. RESULTS AND DISCUSSION

3.1. Synthesis. Herein, block copolymers were prepared, affording flexible, self standing films of dry PEO based polymer electrolytes, which feature sufficient mechanical stability to prevent lithium dendrite growth and reasonable ionic conductivity. A key point is the ability of both blocks to form the so called microphase separated domains on a nanoscale level driven by their polarity difference, i.e., the difference in their mixing parameter χ.[34−36] For this, block copolymers were obtained by first polymerizing the macro monomers **VBmPEOz**, which feature a styrene functionalized mPEOz chain, using DDMAT as a RAFT agent to achieve perfect control over the radical polymerization (Scheme 1). Consequently, a macro RAFT agent[37] based on styrene repeating units with grafted PEO side chains was obtained (**PVBmPEOz**). Subsequently, **PVBmPEOz** was used for the chain extension with styrene to eventually obtain the block copolymer **PVBmPEOz *b* PS** (hereinafter denoted as **BPz**). Three different PEO side chain lengths were employed featuring 8, 22, and 45 EO units corresponding to a mPEOz side chain molar mass of z = 400, 1000, and 2000 g mol^{-1}, respectively. Thus, the degree of polymerization (DP) of **PVBmPEOz** was predefined to be 30 (z = 400), 15 (z = 1000), and 9 (z = 2000) with respect to their different molar mass and their different reactivity. Furthermore, both blocks were matched to feature a final weight ratio of around 50/50, consequently yielding in a total molar mass of ~25, 29, and 38 kg mol^{-1} (as determined by SEC with PS standards, see Table S1) for **BP400**, **BP1000**, and **BP2000**, respectively. This matching was required to obtain flexible, self standing films,

being of particular interest due to the facilitated processing as well as the fact that a dimensionally stable film in principle yields more robust electrode interfaces.[29,38]

3.2. Polymer Electrolytes. The previously described block copolymers **BPz** were used to prepare SPEs with self standing film properties, and the impact of different side chain lengths as well as the LiTFSI content onto the thermal properties and ionic conductivity was studied. Though a detailed description of all of the relationships has been elaborated in previous works,[15,16] we briefly explored the influence of different parameters since it was not clear whether block copolymers behaved in analogy to the previously examined homopolymers.

In this regard, we first chose **BP1000** with a side chain length of around 22 EO units to examine the influence of different LiTFSI concentrations since this side chain length showed promising ionic conductivities in previous studies and featured a medium length among the three different side chains.[15,16,39] SPEs with $[Li^+]/[EO]$ ratios of 1:5, 1:10, 1:15, and 1:20 were produced and investigated using EIS as well as DSC. The latter showed that all LiTFSI concentrations in combination with the side chain approach were sufficient in rendering the PEO domain completely amorphous (Table 1),

Table 1. Overview of the Thermal Properties of the PEO Domains of the Different SPEs

entry	polymer	[LiTFSI]/[EO]	T_g PEO domain (°C)	T_m PEO domain (°C)
1	BP400	1:15	42.2	n/a
2	BP1000	1:5	32.8	n/a
3	BP1000	1:10	43.2	n/a
4	BP1000	1:15	47.2	n/a
5	BP1000	1:20	49.5	n/a
6	BP2000	1:15	47.6	n/a

which is of particular importance since ion transport is suspected to be mainly possible within amorphous domains.[40,41] Furthermore, the glass transition temperature T_g increased with the increasing LiTFSI content due to a higher number of quasi ionic cross links lowering the overall segmental motion of the side chain (Table 1, Figure 2c).[42] Upon inspection of the corresponding ionic conductivities (Figure 2a), it becomes obvious that the $[Li^+]/[EO]$ ratio of 1:5 showed by far the worst ionic conductivity over the whole temperature range. However, all other employed ratios resulted in higher but very similar conductivities over the whole temperature range. A ratio of 1:10 was beneficial at higher temperatures, while the ratios of 1:15 and 1:20 were better at lower temperatures. Overall, we decided to continue the characterization of the SPE with a $[Li^+]/[EO]$ ratio of 1:15 in the following since it exhibited the best overall performance over the whole measured temperature range.

Next, the ionic conductivities of **BP400**, **BP1000**, and **BP2000**, featuring a mPEOz side chain molar mass of z = 400, 1000, and 2000 g mol^{-1}, respectively, comprising a $[Li^+]/[EO]$ ratio of 1:15 were compared. An increasing ionic conductivity over the course from **BP400** to **BP2000** was observed (Figure 2b), likely reflecting the consequences of the side chain approach using styrene as a backbone. Taking **BP400** as an example, around 20 wt % of the PEO domain consists of styrene from the backbone due to the fact that each side chain with around 400 g mol^{-1} features one styrene functionality with around 100 g mol^{-1}. This results in a lower fraction of the PEO domain, which is actually possible to conduct ions, and an increase in T_g due to the significantly higher T_g of styrene in comparison to PEO (Table 1, Figure 2c). These relationships become quite visible when **BP1000** and **BP2000** are included in this consideration. They have a styrene content of 9 and 4.7 wt %, respectively, and, therefore, the percental fraction of styrene content as well as the T_g of the PEO domain is decreasing within this series (Table 1, entry 1, 4 and 6, Figure 2c). Furthermore, longer PEO side chains statistically lead to less intermolecular quasi ionic cross linking in comparison to short side chains, which also impacts T_g.[15,16] Comparing the same LiTFSI ratio, a lower T_g results in higher segmental motion at the same temperature and thus in higher ionic conductivity, as can be seen in Figure 2b. One further explanation for this behavior might be a better phase separation of PS and PEO domains due to a higher difference in polarity when less "backbone PS" contributes to the PEO domain. However, this aspect is difficult to quantify and is beyond the scope of this publication. Furthermore, we noticed that in contrast to our previous study, there was no tradeoff established between the PEO side chain lengths of 1000 and 2000 g mol^{-1}, where one showed higher ionic conductivity at higher temperatures and the other at lower temperatures, respectively.[15] This might be attributed to the block copolymer architecture, which is supposed to form domains on a nanoscale level, hence potentially hindering chain alignment within these domains (thus boosting ionic conductivity for longer chains at lower temperatures). This contrasts with the previously considered homopolymers, where the whole bulk material forms one macroscopic domain.

Still, it has to be noted that the measured ionic conductivities of 1.6×10^{-2} mS cm^{-1}@25 °C and 1.8×10^{-1} mS cm^{-1}@65 °C are relatively low from a practical point of view, but very competitive considering that a truly dry PEO based microphase separated block copolymer having about 50 wt % PS incorporated was used.[30,43,44] In addition, it has to be mentioned that ionic conductivity is only one important feature of an SPE and other properties such as flexibility (Figure 2d) and wettability and thus better interfacial contact to the electrodes, a sufficient electrochemical stability toward the electrodes as well as achieving sufficiently high limiting currents are also highly important for a stable battery performance. Moreover, a high mechanical stability of the SPE and a high limiting current density influences the dendritic growth and thus the cell safety.[45−47] Overall, based on the conductivity results, the SPE prepared from **BP2000** and LiTFSI in a ratio of $[Li^+]/[EO]$ = 1:15 (in the following denoted as **BPE2000**) was further characterized.

3.3. Thermal Characterization and Morphology. One reason for choosing PS as the backbone as well as the block providing the mechanical solidity was due to its high thermal stability.[48] To verify this, a TGA measurement of **BPE2000** was conducted, showing a highly stable SPE with a 5% weight loss at a temperature of 331 °C (T_{d5}) (Figure 3a). The single degradation suggests a simultaneous decomposition of PS, PEO, and LiTFSI, which are all known to decompose around this temperature.[48−50]

Furthermore, we took a closer look at the morphology of **BPE2000**. DSC measurements already showed that micro phase separation took place by revealing a simultaneous appearance of two T_gs for both PS and PEO domains at 100 and −47 °C, respectively (Figure 3b). Furthermore, the ionic conductivities plotted in Figure 2 are only achievable if phase

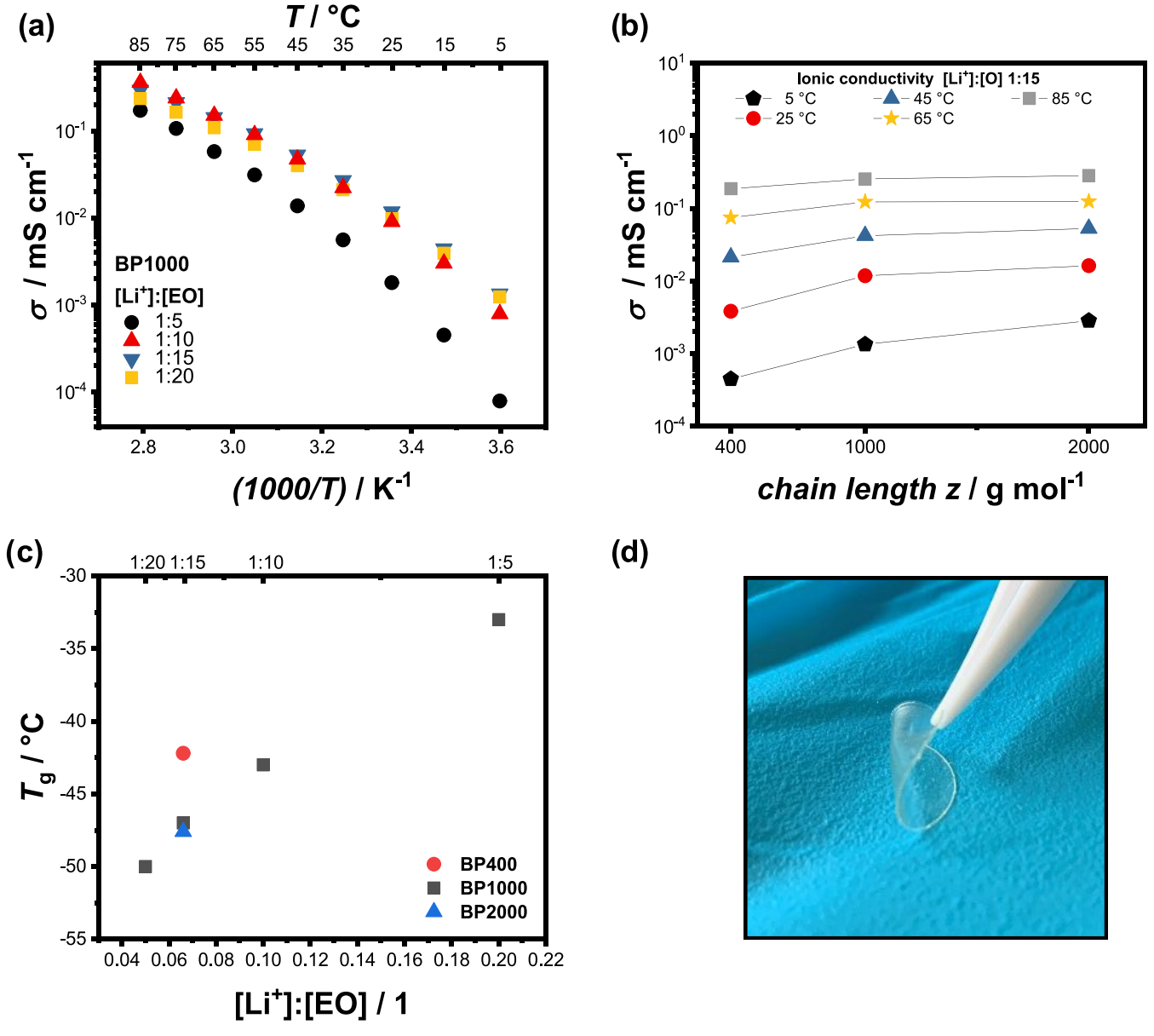

Figure 2. (a) Ionic conductivity of SPEs derived from **BP1000** and different LiTFSI concentrations and (b) comparison of the ionic conductivity of **BP400**, **BP1000**, and **BP2000** featuring a LiTFSI ratio of [Li]/[EO] of 1:15. (c) Corresponding T_gs to (a) and (b). (d) Exemplary picture of the flexible, self standing films.

separation occurred since a nonseparated structure would decrease the ionic conductivity to a significant amount because the conductive domain would contain a substantial amount of a nonconducting polymer, which would increase the T_g and thus decrease the mobility. To further elucidate the morphology, SAXS measurements were conducted (Figure 3c). Herein, the presence of a primary peak at a scattering vector (q) of q^* = 0.23 nm^{-1} confirmed the microphase separation, whereas the presence of further maxima at $2q^*$ and barely visible at $3q^*$ show a high degree of order since nonordered microphase separated polymers only show the main peak.[51] In addition, it is indicative for a lamellar, long range ordered morphology,[52] as anticipated for a block copolymer with a block ratio in the range of 50/50.[27]

$$d = \frac{2\pi}{q^*} \tag{4}$$

Moreover, the average domain spacing (d) of around 27 nm was calculated by eq 4, which is in agreement with comparable PS *b* PEO or PS *b* POEGMA structures featuring a similar molar mass of the blocks (~19 kg mol^{-1} per block),[36,53] though these values are not straightforward to compare because the LiTFSI content and the architecture (linear vs grafted) influence the domain size.[27,54−56]

In addition, rheological measurements of **BPE2000** and the corresponding homopolymer electrolyte (i.e., without the PS block) were conducted (Figure 3d). While the homopolymer electrolyte was a viscous liquid as shown by the low G' and G'' values, **BPE2000** was a self standing film with a G' of around 1 MPa and G'' of around 0.1 MPa. However, it has to be noted that these measured values describe the rheological behavior for the bulk material comprising both PS and PEO domains. Thus, due to the phase separation of the block copolymer, it can be expected that PS domains with their T_g = ~100 °C are predominantly contributing to the mechanical stiffness, which

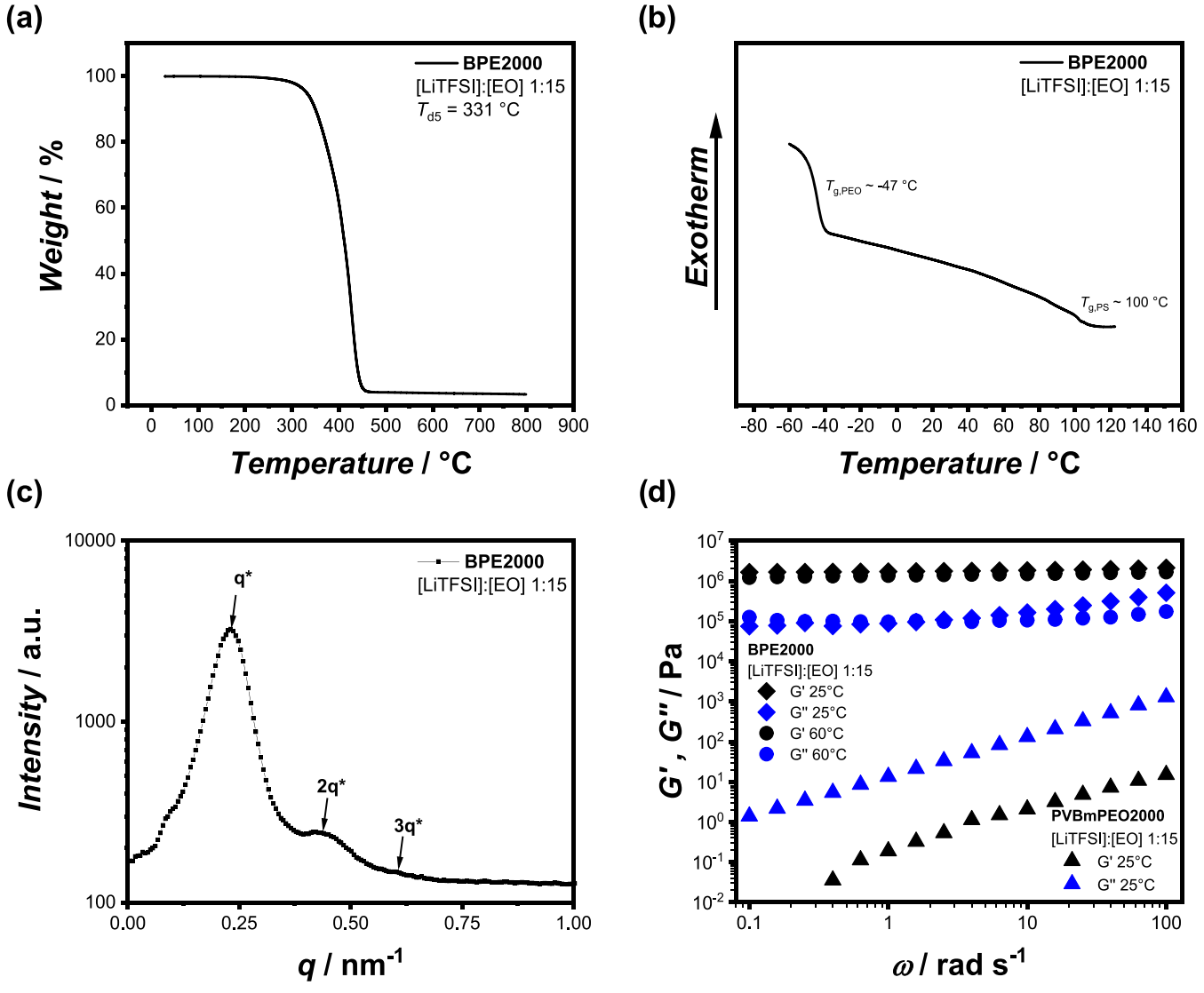

Figure 3. Further characterization of **BPE2000**: (a) TGA thermogram showing a single degradation step, (b) DSC spectrum revealing the phase separation by simultaneously showing the T_g of the PEO and the PS domain, (c) SAXS spectrum suggesting a long range ordered, lamellar morphology, and (d) oscillatory rheology of **BPE2000** and the corresponding homopolymer electrolyte (**PVBmPEO2000**) showing the improved mechanical stability of the bulk material.

is characterized by a G modulus of around 1 GPa.[57] This high mechanical stiffness is even in the range of metallic lithium (G modulus of 3.4 GPa) and is essential regarding the use of **BPE2000** as an SPE in lithium metal batteries to suppress lithium dendrite growth.[45,47,58] Srinivasan et al. proposed that in PEO based polymer electrolytes, a G modulus higher than 3.4 MPa ($G^{SPE} > 10^{-3}$ G^{Li}) leads to plastic deformation of the lithium metal dendrite, thus decreasing the height of the dendrite protrusion and, therefore, additionally decreasing the concentration/overpotential contribution to dendrite growth.[45] Furthermore, PEO domains are characterized by a low T_g and also high flexibility and wettability, which is known for the homopolymer, therefore providing an optimal contact toward the electrodes being equally important.

3.4. Electrochemical Characterization. Since the ionic conductivity of a dual ion conducting SPE is a combination of the anion ($TFSI^-$) and cation (Li^+) mobility and thus only points out the overall ionic conductivity, it is necessary to determine the transference number of such an SPE to obtain an insight into the lithium ion mobility. For this, the combined potentiostatic polarization and complex impedance measurement proposed by Evans et al.[59] was used to determine the transference number of **BPE2000** (Figure 4a). Using eqs 1 and 2, the transference number of **BPE2000** was calculated as 0.13, which is in the typical range for a PEO based SPE[16,43,60,61] and thus further supports the assumption of successful microphase separation and the ion conduction within the PEO domain.

In the next step, we evaluated the electrochemical stability of **BPE2000**, which is an essential information necessary for an intended practical application as an SPE. The intrinsic reductive stability was tested using LSV with copper as a working electrode ranging from 3.0 to 0.5 V vs Li/Li^+. As shown in Figure 4b, a small peak at ~1.5 V as well as a tiny, broad peak at ~0.3−0.5 V was observed, followed by lithium plating below 0 V. Especially, the peak at ~1.5 V is a known phenomenon, yet its origin is not fully understood but reported to be a one time event.[62,63] In fact, CV from 3.0 to 1 V confirmed the presence of this peak only during the first cycle (Figure 4c). In addition, the peak at 0.3 V seemed to decrease during cycles.

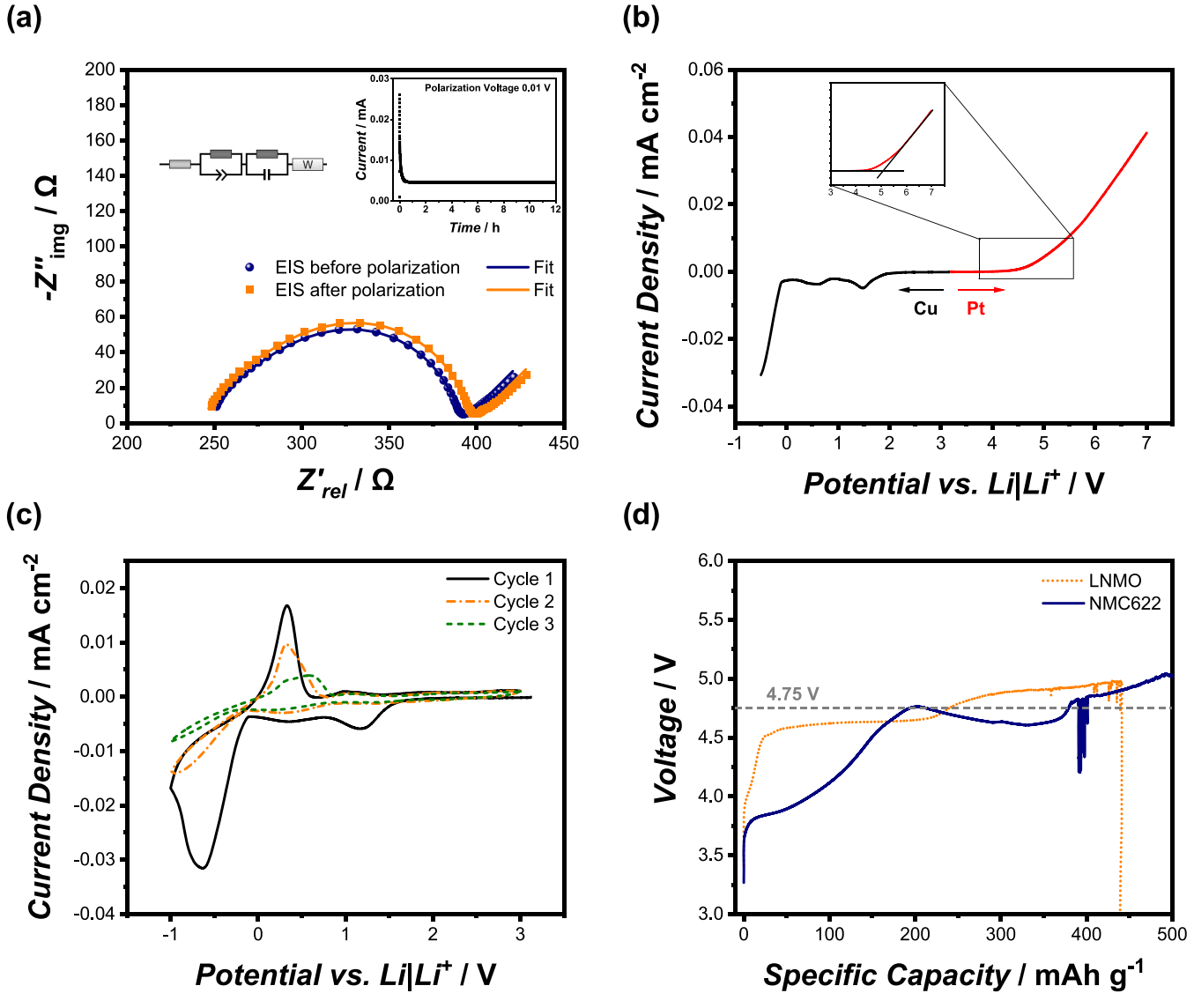

Figure 4. (a) Chronoamperometry and EIS of **BPE2000** determining the transference number. Determination of the electrochemical stability of **BPE2000** by (b) linear sweep voltammetry (LSV) in a range from −0.5 to 7.0 V (0.1 mV s^{-1}), (c) CV in a range from −1.0 to 3.0 V (0.1 mV s^{-1}) and (d) galvanostatic overcharging (0.1C) using LNMO and NMC622 as high voltage cathode materials.

Moreover, the intrinsic oxidative stability of the SPE using an anodic sweep from 3.0 to 7.0 V was determined as 5.1 V vs Li/Li^+ with platinum serving as the working electrode (Figure 4b). However, these values are highly dependent on the set limits. Often, 0.01 or 0.015 mA cm^{-2} are chosen,[64] corresponding to even higher values. Still, the electrochemical stability window measured on inert materials such as platinum or copper does not reflect a realistic behavior in a lithium metal battery. High surface area cathodes and chemical reactive lithium metal often support electrochemical degradation during cycling.[20,62] Therefore, to further investigate the compatibility with high voltage cathode materials, galvanostatic overcharging of the positive electrode was performed to determine limiting potentials in a more realistic way (Figure 4d). Commonly employed LNMO as well as NMC622 were used as high voltage cathode materials to determine the onset of oxidation. Independent of the different mechanisms of lithium de /intercalation, a characteristic voltage plateau at 4.75 V vs $Li|Li^+$ was observed for both LNMO and NMC622 cathodes. This voltage plateau reflects parasitic reactions originating from the oxidative decomposition of either the SPE itself, the present PVdF in the composite cathode, or both.[65] As mentioned above, the onset of oxidative decomposition of the SPE against active materials can differ from the decomposition against inert materials such as platinum or copper. Nonetheless, there is no apparent current (<0.01 mA cm^{-2} for potentiodynamic and no obvious voltage plateau for galvanostatic measurement) evolving from electro lyte oxidation below 4.3 V vs $Li|Li^+$ for both potentiodynamic and galvanostatic measurements and, therefore, an application of this SPE using high voltage cathode materials such as NMC622 appears very likely.

Since one of the major advantages of all solid state batteries (ASSB) is the use of lithium metal, resulting in an increased energy density, it is essential that the solid state electrolyte is suitable for use against lithium metal electrodes.[3,66] Moreover, the increased mechanical stability due to the PS block (vide supra) is beneficial for the inhibition of lithium dendritic growth. Therefore, lithium plating stripping experiments were conducted at a current density of 0.1 mA cm^{-2} to examine the

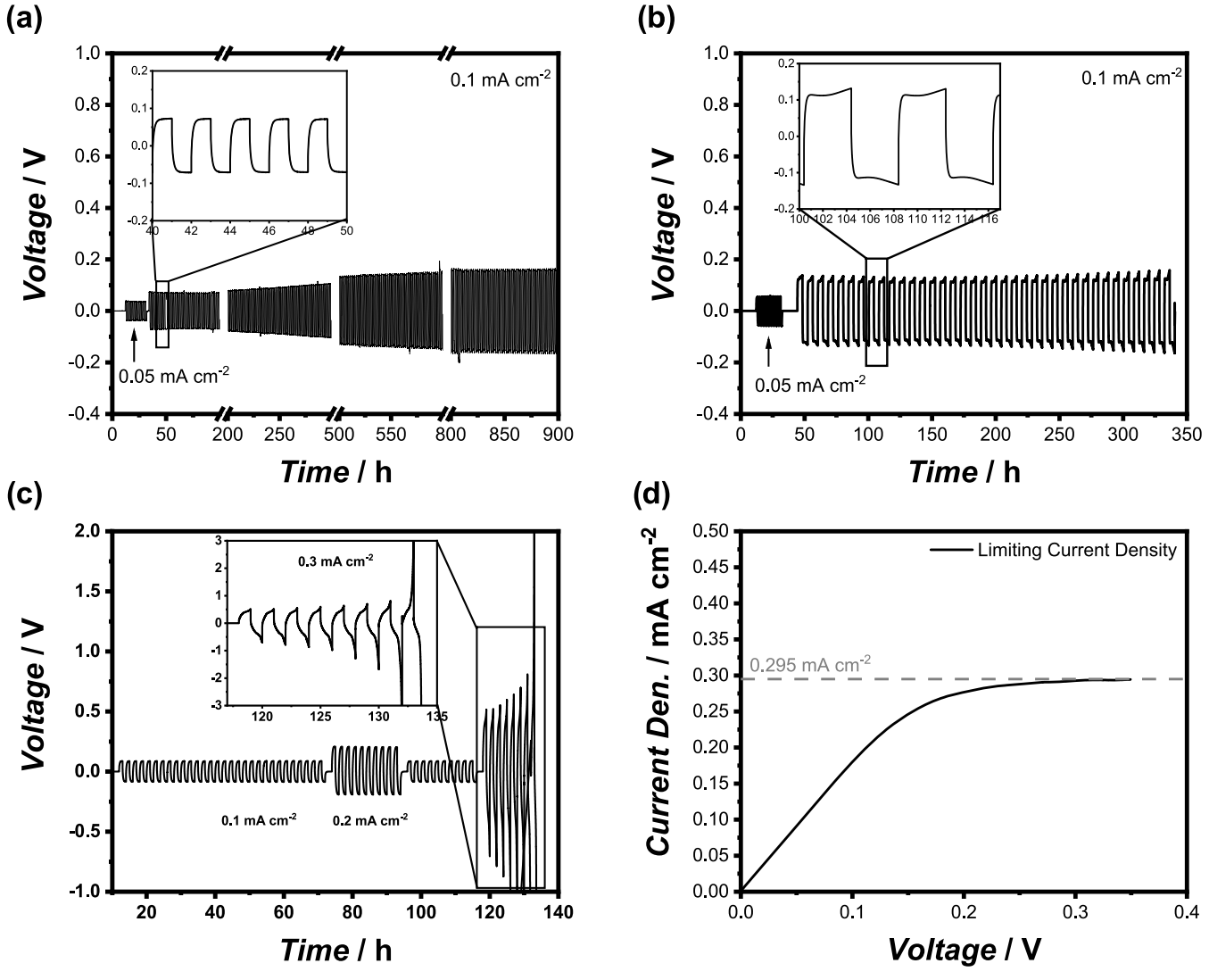

Figure 5. Lithium plating stripping experiments. (a) Conditioning using 0.05 mA cm^{-2} for 10 cycles. Afterward, lithium was constantly plated and stripped with a current density of 0.1 mA cm^{-2} for 1 h over a total of 1000 h (b) Conditioning using 0.05 mA cm^{-2} for 10 cycles. Afterward, lithium was constantly plated and stripped with a current density of 0.1 mA cm^{-2} for 4 h over a total of 296 h. (c) Lithium plating stripping with alternating current densities with 10 cycles at 0.1 mA cm^{-2} in between and (d) LSV measurement in a Li|Li cell with a sweep rate of 0.02 mV s^{-1} to identify the limiting current density derived from the plateau.

interfacial long term stability of lithium metal and the ability to reduce lithium dendrite growth. As shown in Figure 5a, the overvoltage (initial overvoltage ~0.075 V) increased within the first cycles, reflecting an increase of the resistance, presumably originating from the formation of an additional SEI by insignificant electrolyte decomposition. Once the SEI layer was completely formed, the overvoltage remained nearly stable at ~0.15 V over thousand hours. In general, this long term overvoltage of ~0.15 V is in the normal range in comparison to similar PEO based SPEs, whereas the initial overvoltage of ~0.075 V is rather low[43,67] Though, overvoltages in Li|SPE|Li cells are strongly related to several polymer properties such as film dimensions, interface resistances, or mechanical proper ties, which makes it a complex parameter and thus it is not trivial to directly compare different SPEs. Moreover, the shape of the voltage profiles (see the inset of Figure 5a) was rapidly reaching a plateau, implying a reduced cell polarization due to ionic concentration gradients.[62] These findings indicated a stable and homogeneous lithium deposition behavior, and consequently no short circuit by dendrite penetration was observed over thousand hours, whereas comparable PS PEO block copolymers already underwent a short circuit after 240 h[43] and pure PEO even in <40 h[67] under the same current density.

To further investigate the lithium dendrite growth, plating and stripping experiments were performed with a longer plating and stripping time (Figure 5b) as well as alternating current densities (Figure 5c).

As shown in Figure 5b, the plating and stripping time with a current density of 0.1 mA cm^{-2} was extended to 4 h. Similar to Figure 5a, the voltage plateau at ~0.1 V was rapidly reached and remained nearly constant for around 3 h, thus no cell polarization could be found, implying a stable lithium deposition behavior. Afterward, a small increase in overvoltage was observed (see the inset of Figure 5b), probably resulting from kinetic limitations, possibly leading to slowly growing lithium dendrites. However, this polarization seems to be reversible and does not result in a rapid cell failure or short circuit as can be seen from the stable long term overvoltage,

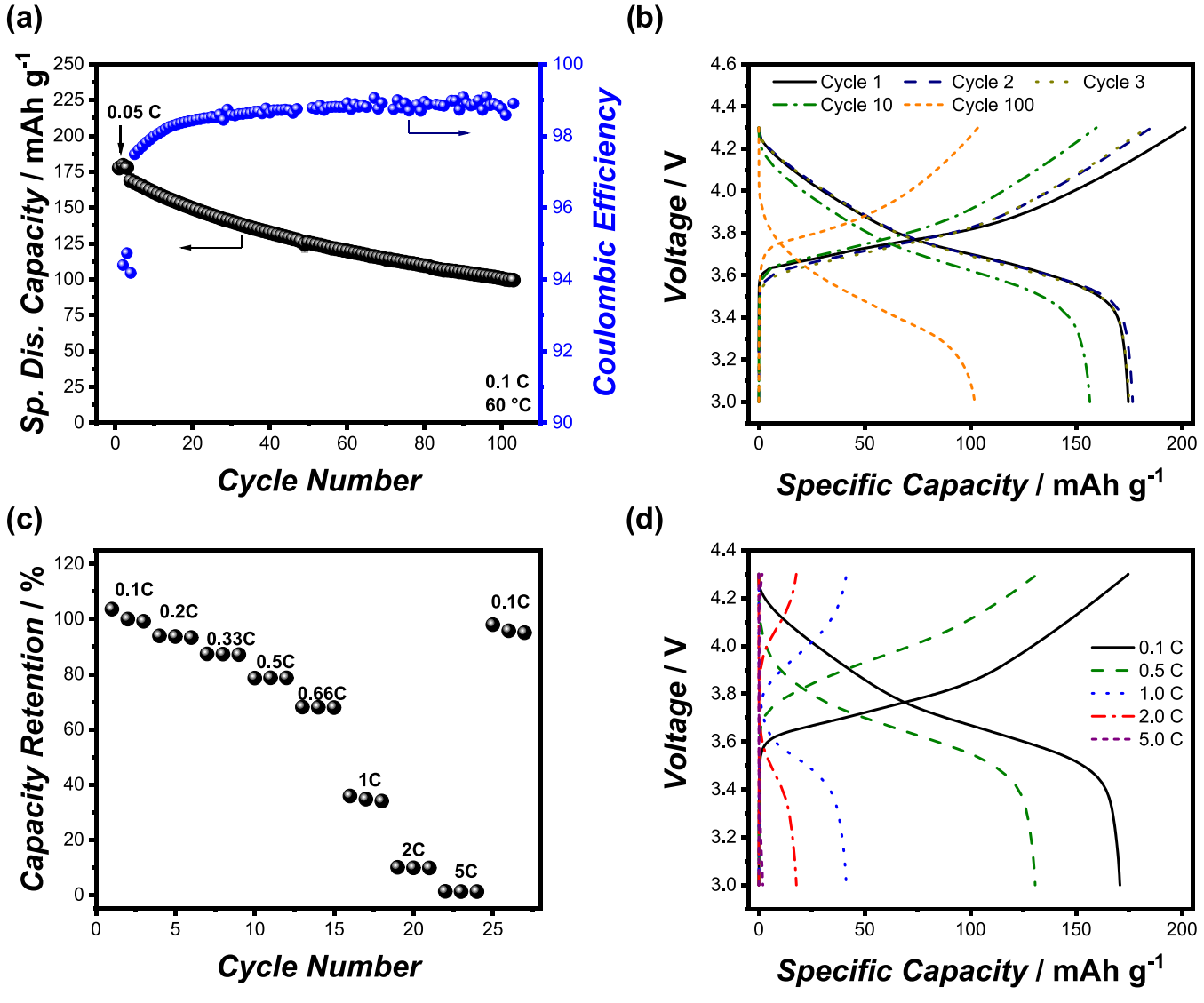

Figure 6. (a) Constant current cycling at 0.1C and (c) rate capability tests (varying charge rate; 100% corresponds to ~172 mAh g^{-1}) of Li|BPE2000|NMC622 cells at 60 °C. Selected charge and discharge profiles of (b) different cycles as well as (d) different C rates. Notably, no voltage noise or rapid cell failure is observed.

which showed only a small increase over ~300 h (see also the corresponding EIS data Figure S8).

Moreover, the influence of different current densities (Figure 5c) was evaluated by gradually increasing the latter from 0.1 to 0.3 mA cm^{-2} in intervals of 10 cycles. In addition, between the two intervals, the cell was allowed to cycle for 10 cycles at 0.1 mA cm^{-2}. As summarized in Figure 5c, it was found that by applying a current density of 0.3 mA cm^{-2}, the overall overvoltage quickly increased and a severe polarization during one cycle (see the inset of Figure 5c) was observed, whereas a stable voltage plateau at 0.1 and 0.25 V was reached for current densities of 0.1 and 0.2 mA cm^{-2}, respectively. This polarization originated from concentration gradients within the electrolyte as a result of an insufficient Li^+ transport and resulted in a considerable dendrite growth that cannot be suppressed by the morphology, hence, yielding a cell failure for current densities higher than 0.3 mA cm^{-2}. However, compared to a pure PEO based SPE, where a short circuit is quickly observed at 0.2 mA cm^{-2}, the limiting current density shown here is significantly increased, although the ionic conductivity is lower.[68]

To corroborate the current density limitations derived from plating and stripping experiments, LSV was conducted with symmetrical Li|SPE|Li cells (Figure 5d). The plateau at a current density of ~0.3 mA cm^{-2} is assumed as the limiting current density and is in good agreement with the current density limitations previously identified in plating and stripping experiments. As indicated before, the limiting current density is higher compared to literature known PEO based SPEs comprising comparable or even significantly higher ionic conductivities, thus underlining the beneficial interplay between mechanical stability provided by the PS domain, resulting in the ability to suppress dendritic growth and the ion conduction derived from the PEO domain once more.[68−70]

3.5. Galvanostatic Cycling and Rate Capability. After the promising results regarding the electrochemical stability against high voltage cathodes as well as stable Li|SPE interfaces, long term constant current cycling and rate capability tests were conducted in Li|NMC622 full cells.

Constant current cycling was performed at 60 °C and a rate of 0.1C (Figure 6a, corresponding EIS data Figure S9). Remarkably, neither a rapid cell failure nor a commonly described voltage noise, both usually associated with PEO based PEs and NMC622,[19−21] was observed over the course of 100 cycles (Figure 6b). These results strongly support the recently revised point of view regarding the use of PEO based electrolytes in combination with NMC cathodes. Homann et al. showed that the voltage noise/rapid cell failure might not be caused by an insufficient oxidative stability but rather reflect insufficient mechanical stability and eventually Li dendrite penetration.[19] However, if sufficient mechanical stability[20,21] or electrolyte thickness (e.g., 800 μm)[19] is provided, dendrite penetration (and thus voltage noise and rapid cell failure) are suppressed or prolonged, respectively. Though the employed **BPE2000** films featured a thickness of only ∼100 μm, the available mechanical stability (G' = 1 MPa for the bulk material, up to G' = 1 GPa within the PS domain) due to the PS domain allowed for the successful cycling in Li||NMC622 full cells, thus supporting the statement that PEO based SPEs can be used with NMC622, as long as a sufficient mechanical stability is guaranteed. Nonetheless, the cells did still show a noticeable capacity fading in comparison to other reports concerning non PEO based SPE classes in combination with NMC.[64] However, each SPE class features its own advantages and disadvantages in terms of performance and also availability and affordability, thus complicating direct comparison. Still, the origin of the capacity fading needs to be evaluated in more detail in upcoming studies targeting an efficient cycling of PEO based PEs in Li||NMC622 cells.

In addition, the rate capability was evaluated by varying the charge rate, while the discharge rate was kept constant at 0.1C. At 0.5C, the cells retain 80% of the initial specific capacity and a severe decrease of the capacity retention merely occurred at C rates higher than 0.66C (Figure 6c,d), which is in good agreement with the measured limiting current density, yielding sufficient capacity retention until a current density of ∼164 mA g^{-1} (180 mA g^{-1} = 1C). The provided ionic conductivity of the PEO based electrolytes was too low to enable a sufficient Li^+ transport at higher C rates. Here, probably kinetic limitations resulted in a blocking type polarization and thus a massive decrease in available capacity. This behavior can be seen in Figure 6d, where a steep voltage increase is visible for 1, 2, and 5C without a noticeable gain in capacity.[70] Nevertheless, even at those high C rates neither voltage noise nor rapid cell failure was observed, as shown in Figure 6d, once more documenting the enormous potential of **BPE2000**.

To overcome the capacity fading as well as the limited C rate capability in the first instance, it is necessary to enhance the ionic conductivity of **BPE2000**. For this, the implementation of additives such as plasticizers is one of the most applied approaches to do so.[5,11,12,62] However, for bulk materials, plasticizers not only increase the mobility of chains (and thus decrease the T_g) but also decrease the mechanical stability as a consequence, resulting again in issues with accelerated lithium dendrite growth. In this regard, block copolymers such as **BP2000** can be designed in a sophisticated way allowing for the selective implementation of plasticizers into the PEO domain while maintaining an untouched PS domain, thus—when properly balanced—resulting in an increased ionic conductivity without a decreased mechanical stability. This possibility, in combination with the straightforward synthesis of the styrene based PEO side chain block copolymers, shows once more the huge potential of this material since it allows for a simple decoupling of the implementation of additives and mechanical stability being otherwise hardly achievable. Thus, we will focus on optimizing the here presented SPE using nonvolatile additives to enhance the ionic conductivity while still featuring a dry SPE.

4. CONCLUSIONS

Herein, we introduced the straightforward synthesis of an inexpensive and fully dry polymer electrolyte based on styrene, featuring PEO side chains overcoming both common drawbacks of comparable systems, namely, on the one hand, the tedious synthesis of PS *b* PEO and, on the other hand, the insufficient stability of PS *b* POEGMA block copolymers. The special architecture allowed to (a) reduce crystallization, (b) enable a microphase separation with long range order, resulting in (c) a good mechanical stability (G' = 1 MPa for the bulk material, up to G' = 1 GPa within the PS domain) and (d) a good ionic conductivity decoupled from the mechanical stability. First, the impact of different LiTFSI ratios as well as different side chain lengths on the ionic conductivity and the thermal properties was briefly examined, showing that a [LiTFSI]/[EO] ratio of 1:15 and relatively long side chain with around 45 EO repeating units exhibited a reasonably high ionic conductivity of 1.6 × 10^{-2} mS cm^{-1}@25 °C. Subsequently, an SPE comprising the highest ionic conductivity was further analyzed in detail. We could show that the PS and PEO domains are separated on a microscopic level forming a long range ordered, most probably lamellar block copolymer morphology, allowing for the preparation of an overall flexible, self standing film, featuring a good mechanical stability provided by the high modulus PS domains as well as a wettability provided by the low modulus PEO domains.

A sufficient oxidative stability at voltages beyond 4.75 V was found using both potentiostatic and galvanostatic techniques as well as different electrodes and active materials, thus demonstrating relevant compatibility with high voltage cathode materials such as NMC622. A stable Li|SPE interface was established from LSV/CV as well as lithium stripping/plating tests over 1000 h and a comparable high limiting current density of 0.3 mA cm^{-2} was in respect to the provided ionic conductivity derived as a consequence of improved mechanical stability. Full cell cycling in Li||NMC622 cells did not show any indication of rapid cell failure or the presence of voltage noise, unlike previously associated with PEO based SPEs and NMC622, thus supporting the recently proposed opinion that sufficient mechanical stability is necessary for PEO based SPEs to be applicable in combination with high voltage cathodes, such as NMC622. Moreover, we showed that such microphase separated PEO based SPEs are of high interest for the next generation of high voltage lithium metal batteries, providing a straightforward and inexpensive approach for polymer based energy storage solutions. In contrast to Bolloré's state of the art LMP technology, the replacement of LFP with high voltage cathodes such as NMC622 increases the ASSB performance in terms of energy density and costs and thus might push the applicability of SPEs in ASSB, a major step forward.[6] Nonetheless, the present SPE is still limited by its ionic conductivity in a practical point of view and noticeable capacity fading in combination with NMC622. To overcome this issue, further studies focusing on the enhancement of the ionic conductivity while maintaining all of the other beneficial properties are currently underway. This will not only allow for

higher C rates but also enable long term cycling at lower temperatures, thereby circumventing parasitic processes. Moreover, the origin of capacity fading should be examined to drive forward the application of inexpensive PEO based SPEs in high voltage lithium metal batteries.

■ ASSOCIATED CONTENT

● Supporting Information

The Supporting Information is available free of charge at https://pubs.acs.org/doi/10.1021/acsami.1c08841.

Exemplary ^{1}H NMR and ^{13}C NMR spectra; overview of the different block copolymers; SEC of chain extension; additional TGA thermograms; pictures of **BPE2000** films; EIS data of Li|BPE2000|Li and Li|BPE2000|NMC622 cells (PDF)

■ AUTHOR INFORMATION

Corresponding Authors

Gunther Brunklaus − *Helmholtz Institute Münster, IEK 12, Forschungszentrum Jülich GmbH, 48149 Münster, Germany; MEET Battery Research Center/Institute of Physical Chemistry, University of Münster, 48149 Münster, Germany;* orcid.org/0000 0003 0030 1383; Email: g.brunklaus@fz juelich.de

Patrick Théato − *Karlsruhe Institute of Technology (KIT), Institute for Chemical Technology and Polymer Chemistry (ITCP), 76131 Karlsruhe, Germany; Karlsruhe Institute of Technology (KIT), Soft Matter Laboratory—Institute for Biological Interfaces III (IBG 3), 76344 Eggenstein Leopoldshafen, Germany;* orcid.org/0000 0002 4562 9254; Email: patrick.theato@kit.edu

Authors

Andreas J. Butzelaar − *Karlsruhe Institute of Technology (KIT), Institute for Chemical Technology and Polymer Chemistry (ITCP), 76131 Karlsruhe, Germany;* orcid.org/0000 0002 0843 2719

Philipp Röring − *Helmholtz Institute Münster, IEK 12, Forschungszentrum Jülich GmbH, 48149 Münster, Germany*

Tim P. Mach − *Karlsruhe Institute of Technology (KIT), Institute for Chemical Technology and Polymer Chemistry (ITCP), 76131 Karlsruhe, Germany*

Maxi Hoffmann − *Karlsruhe Institute of Technology (KIT), Institute for Chemical Technology and Polymer Chemistry (ITCP), 76131 Karlsruhe, Germany*

Fabian Jeschull − *Karlsruhe Institute of Technology (KIT), Institute for Applied Materials—Energy Storage Systems (IAM ESS), 76344 Eggenstein Leopoldshafen, Germany;* orcid.org/0000 0002 5927 1978

Manfred Wilhelm − *Karlsruhe Institute of Technology (KIT), Institute for Chemical Technology and Polymer Chemistry (ITCP), 76131 Karlsruhe, Germany;* orcid.org/0000 0003 2105 6946

Martin Winter − *Helmholtz Institute Münster, IEK 12, Forschungszentrum Jülich GmbH, 48149 Münster, Germany; MEET Battery Research Center/Institute of Physical Chemistry, University of Münster, 48149 Münster, Germany*

Complete contact information is available at: https://pubs.acs.org/10.1021/acsami.1c08841

Author Contributions

[#]A.J.B. and P.R. contributed equally to this work.

Author Contributions

A.J.B.: Conceptualization, Investigation, and Writing—Original Draft. P.R.: Conceptualization, Investigation, and Writing—Original Draft. T.P.M.: Investigation. M.H.: Investigation. F.J.: Supervision. M.W.: Writing—Review & Editing, Supervision. M.W.: Supervision and Funding acquisition. G.B.: Writing—Review & Editing, Supervision, and Funding acquisition. P.T.: Conceptualization, Writing—Review & Editing, Supervision, and Funding acquisition.

Notes

The authors declare no competing financial interest.

■ ACKNOWLEDGMENTS

Financial support from the German Federal Ministry of Education and Research (BMBF) within "FestBatt" (13XP0175A and 13XP0175C) is gratefully acknowledged. M.H. gratefully acknowledges support from the "Stiftung der Deutschen Wirtschaft (sdw)" within the Klaus Murmann fellowship. The authors thank Dr. J. Binder from Karlsruher Institute of Technology (KIT), Institute for Applied Materials (Prof. H. Ehrenberg), for kindly providing LMNO samples.

■ REFERENCES

(1) Blomgren, G. E. The Development and Future of Lithium Ion Batteries. *J. Electrochem. Soc.* **2017**, *164*, A5019−A5025.

(2) Grey, C. P.; Hall, D. S. Prospects for lithium ion batteries and beyond a 2030 vision. *Nat. Commun.* **2020**, *11*, No. 6279. Published Online: Dec. 8, 2020.

(3) Cheng, X. B.; Zhang, R.; Zhao, C. Z.; Zhang, Q. Toward Safe Lithium Metal Anode in Rechargeable Batteries: A Review. *Chem. Rev.* **2017**, *117*, 10403−10473. Published Online: Jul. 28, 2017.

(4) Aziz, S. B.; Woo, T. J.; Kadir, M. F. Z.; Ahmed, H. M. A conceptual review on polymer electrolytes and ion transport models. *J. Sci.: Adv. Mater. Devices* **2018**, *3*, 1−17.

(5) Xue, Z.; He, D.; Xie, X. Poly(ethylene oxide) based electrolytes for lithium ion batteries. *J. Mater. Chem. A* **2015**, *3*, 19218−19253.

(6) Varzi, A.; Thanner, K.; Scipioni, R.; Di Lecce, D.; Hassoun, J.; Dörfler, S.; Altheus, H.; Kaskel, S.; Prehal, C.; Freunberger, S. A. Current status and future perspectives of lithium metal batteries. *J. Power Sources* **2020**, *480*, No. 228803.

(7) Zhang, H.; Eshetu, G. G.; Judez, X.; Li, C.; Rodriguez Martínez, L. M.; Armand, M. Electrolyte Additives for Lithium Metal Anodes and Rechargeable Lithium Metal Batteries: Progress and Perspectives. *Angew. Chem., Int. Ed.* **2018**, *57*, 15002−15027. Published Online: Oct. 15, 2018.

(8) Zhu, L.; Li, J.; Jia, Y.; Zhu, P.; Jing, M.; Yao, S.; Shen, X.; Li, S.; Tu, F. Toward high performance solid state lithium ion battery with a promising PEO / PPC blend solid polymer electrolyte. *Int. J. Energy Res.* **2020**, *44*, 10168−10178.

(9) Devaux, D.; Bouchet, R.; Glé, D.; Denoyel, R. Mechanism of ion transport in PEO/LiTFSI complexes: Effect of temperature, molecular weight and end groups. *Solid State Ionics* **2012**, *227*, 119−127.

(10) Zhang, Y.; Lu, W.; Cong, L.; Liu, J.; Sun, L.; Mauger, A.; Julien, C. M.; Xie, H.; Liu, J. Cross linking network based on Poly(ethylene oxide): Solid polymer electrolyte for room temperature lithium battery. *J. Power Sources* **2019**, *420*, 63−72.

(11) Das, S.; Ghosh, A. Ionic conductivity and dielectric permittivity of PEO LiClO 4 solid polymer electrolyte plasticized with propylene carbonate. *AIP Adv.* **2015**, *5*, No. 27125.

(12) Banitaba, S. N.; Semnani, D.; Heydari Soureshjani, E.; Rezaei, B.; Ensafi, A. A. The effect of concentration and ratio of ethylene carbonate and propylene carbonate plasticizers on characteristics of the electrospun PEO based electrolytes applicable in lithium ion batteries. *Solid State Ionics* **2020**, *347*, No. 115252.

(13) Xu, L.; Li, J.; Deng, W.; Li, L.; Zou, G.; Hou, H.; Huang, L.; Ji, X. Boosting the ionic conductivity of PEO electrolytes by waste eggshell derived fillers for high performance solid lithium/sodium batteries. *Mater. Chem. Front.* **2021**, *5*, 1315−1323.
(14) Patla, S. K.; Ray, R.; Asokan, K.; Karmakar, S. Investigation of ionic conduction in PEO−PVDF based blend polymer electrolytes. *J. Appl. Phys.* **2018**, *123*, No. 125102.
(15) Butzelaar, A. J.; Liu, K. L.; Röring, P.; Brunklaus, G.; Winter, M.; Theato, P. A Systematic Study of Vinyl Ether Based Poly (Ethylene Oxide) Side Chain Polymer Electrolytes. *ACS Appl. Polym. Mater.* **2021**, *3*, 1573−1582.
(16) Rosenbach, D.; Mödl, N.; Hahn, M.; Petry, J.; Danzer, M. A.; Thelakkat, M. Synthesis and Comparative Studies of Solvent Free Brush Polymer Electrolytes for Lithium Batteries. *ACS Appl. Energy Mater.* **2019**, *2*, 3373−3388.
(17) Butzelaar, A. J.; Gauthier Jaques, M.; Liu, K. L.; Brunklaus, G.; Winter, M.; Theato, P. The Power of Architecture − Cage shaped PEO and its Application as a Polymer Electrolyte. *Polym. Chem.* **2021**, *12*, No. 4326.
(18) Arya, A.; Sharma, A. L. Polymer electrolytes for lithium ion batteries: a critical study. *Ionics* **2017**, *23*, 497−540.
(19) Homann, G.; Stolz, L.; Nair, J.; Laskovic, I. C.; Winter, M.; Kasnatscheew, J. Poly(Ethylene Oxide) based Electrolyte for Solid State Lithium Batteries with High Voltage Positive Electrodes: Evaluating the Role of Electrolyte Oxidation in Rapid Cell Failure. *Sci. Rep.* **2020**, *10*, No. 4390. Published Online: Mar. 9, 2020.
(20) Homann, G.; Stolz, L.; Neuhaus, K.; Winter, M.; Kasnatscheew, J. Effective Optimization of High Voltage Solid State Lithium Batteries by Using Poly(ethylene oxide) Based Polymer Electrolyte with Semi Interpenetrating Network. *Adv. Funct. Mater.* **2020**, *30*, No. 2006289.
(21) Homann, G.; Stolz, L.; Winter, M.; Kasnatscheew, J. Elimination of "Voltage Noise" of Poly (Ethylene Oxide) Based Solid Electrolytes in High Voltage Lithium Batteries: Linear versus Network Polymers. *iScience* **2020**, *23*, No. 101225. Published Online: Jun. 3, 2020.
(22) Wetjen, M.; Kim, G. T.; Joost, M.; Appetecchi, G. B.; Winter, M.; Passerini, S. Thermal and electrochemical properties of PEO LiTFSI Pyr14TFSI based composite cathodes, incorporating 4 V class cathode active materials. *J. Power Sources* **2014**, *246*, 846−857.
(23) Phan, T. N. T.; Issa, S.; Gigmes, D. Poly(ethylene oxide) based block copolymer electrolytes for lithium metal batteries. *Polym. Int.* **2019**, *68*, 7−13.
(24) Sethuraman, V.; Mogurampelly, S.; Ganesan, V. Ion transport mechanisms in lamellar phases of salt doped PS PEO block copolymer electrolytes. *Soft Matter* **2017**, *13*, 7793−7803.
(25) Bouchet, R.; Phan, T. N. T.; Beaudoin, E.; Devaux, D.; Davidson, P.; Bertin, D.; Denoyel, R. Charge Transport in Nanostructured PS−PEO−PS Triblock Copolymer Electrolytes. *Macromolecules* **2014**, *47*, 2659−2665.
(26) Yuan, R.; Teran, A. A.; Gurevitch, I.; Mullin, S. A.; Wanakule, N. S.; Balsara, N. P. Ionic Conductivity of Low Molecular Weight Block Copolymer Electrolytes. *Macromolecules* **2013**, *46*, 914−921.
(27) Chintapalli, M.; Le, T. N. P.; Venkatesan, N. R.; Mackay, N. G.; Rojas, A. A.; Thelen, J. L.; Chen, X. C.; Devaux, D.; Balsara, N. P. Structure and Ionic Conductivity of Polystyrene block poly(ethylene oxide) Electrolytes in the High Salt Concentration Limit. *Macro molecules* **2016**, *49*, 1770−1780.
(28) Singh, M.; Odusanya, O.; Wilmes, G. M.; Eitouni, H. B.; Gomez, E. D.; Patel, A. J.; Chen, V. L.; Park, M. J.; Fragouli, P.; Iatrou, H.; Hadjichristidis, N.; Cookson, D.; Balsara, N. P. Effect of Molecular Weight on the Mechanical and Electrical Properties of Block Copolymer Electrolytes. *Macromolecules* **2007**, *40*, 4578−4585.
(29) Rolland, J.; Brassinne, J.; Bourgeois, J. P.; Poggi, E.; Vlad, A.; Gohy, J. F. Chemically anchored liquid PEO based block copolymer electrolytes for solid state lithium ion batteries. *J. Mater. Chem. A* **2014**, *2*, 11839−11846.
(30) Devaux, D.; Glé, D.; Phan, T. N. T.; Gigmes, D.; Giroud, E.; Deschamps, M.; Denoyel, R.; Bouchet, R. Optimization of Block Copolymer Electrolytes for Lithium Metal Batteries. *Chem. Mater.* **2015**, *27*, 4682−4692.
(31) Bergfelt, A.; Rubatat, L.; Brandell, D.; Bowden, T. Poly(benzyl methacrylate) poly[(oligo ethylene glycol) methyl ether methacry late] triblock copolymers as solid electrolyte for lithium batteries. *Solid State Ionics* **2018**, *321*, 55−61.
(32) Rieger, J. The glass transition temperature of polystyrene. *J. Therm. Anal.* **1996**, *46*, 965−972.
(33) Mereacre, V.; Stüble, P.; Ghamlouche, A.; Binder, J. R. Enhancing the Stability of LiNi0.5Mn1.5O4 by Coating with LiNbO3 Solid State Electrolyte: Novel Chemically Activated Coating Process versus Sol Gel Method. *Nanomaterials* **2021**, *11*, No. 548. Published Online: Feb. 22, 2021.
(34) Olvera de la Cruz, M. Theory of microphase separation in block copolymer solutions. *J. Chem. Phys.* **1989**, *90*, 1995−2002.
(35) Zhang, J.; Yu, X.; Yang, P.; Peng, J.; Luo, C.; Huang, W.; Han, Y. Microphase separation of block copolymer thin films. *Macromol. Rapid Commun.* **2010**, *31*, 591−608. Published Online: Jan. 18, 2010.
(36) Gartner, T. E.; Kubo, T.; Seo, Y.; Tansky, M.; Hall, L. M.; Sumerlin, B. S.; Epps, T. H. Domain Spacing and Composition Profile Behavior in Salt Doped Cyclic vs Linear Block Polymer Thin Films: A Joint Experimental and Simulation Study. *Macromolecules* **2017**, *50*, 7169−7176.
(37) Yu, M.; Tan, J.; Yang, J.; Zeng, Z. Z type and R type macro RAFT agents in RAFT dispersion polymerization − another mechanism perspective on PISA. *Polym. Chem.* **2016**, *7*, 3756−3765.
(38) Krause, C. H.; Butzelaar, A. J.; Diddens, D.; Dong, D.; Théato, P.; Bedrov, D.; Hwang, B. J.; Winter, M.; Brunklaus, G. Quasi solid single ion conducting polymer electrolyte membrane containing novel fluorinated poly(arylene ether sulfonimide) for lithium metal batteries. *J. Power Sources* **2021**, *484*, No. 229267.
(39) Itoh, T.; Fujita, K.; Uno, T.; Kubo, M. Polymer electrolytes based on vinyl ethers with various EO chain length and their polymer electrolytes cross linked by electron beam irradiation. *Ionics* **2017**, *23*, 257−264.
(40) Cheng, S.; Li, X.; Zheng, Y.; Smith, D. M.; Li, C. Y. Anisotropic ion transport in 2D polymer single crystal based solid polymer electrolytes. *Giant* **2020**, *2*, No. 100021.
(41) Borodin, O.; Smith, G. D. Mechanism of Ion Transport in Amorphous Poly(ethylene oxide)/LiTFSI from Molecular Dynamics Simulations. *Macromolecules* **2006**, *39*, 1620−1629.
(42) Lascaud, S.; Perrier, M.; Vallee, A.; Besner, S.; Prud'homme, J.; Armand, M. Phase Diagrams and Conductivity Behavior of Poly (ethylene oxide) Molten Salt Rubbery Electrolytes. *Macromolecules* **1994**, *27*, 7469−7477.
(43) Zhang, B.; Zhang, Y.; Zhang, N.; Liu, J.; Cong, L.; Liu, J.; Sun, L.; Mauger, A.; Julien, C. M.; Xie, H.; Pan, X. Synthesis and interface stability of polystyrene poly(ethylene glycol) polystyrene triblock copolymer as solid state electrolyte for lithium metal batteries. *J. Power Sources* **2019**, *428*, 93−104.
(44) Wang, C.; Sakai, T.; Watanabe, O.; Hirahara, K.; Nakanishi, T. All Solid State Lithium Polymer Battery Using a Self Cross Linking Polymer Electrolyte. *J. Electrochem. Soc.* **2003**, *150*, No. A1166.
(45) Barai, P.; Higa, K.; Srinivasan, V. Lithium dendrite growth mechanisms in polymer electrolytes and prevention strategies. *Phys. Chem. Chem. Phys.* **2017**, *19*, 20493−20505.
(46) Bai, P.; Li, J.; Brushett, F. R.; Bazant, M. Z. Transition of lithium growth mechanisms in liquid electrolytes. *Energy Environ. Sci.* **2016**, *9*, 3221−3229.
(47) Monroe, C.; Newman, J. Dendrite Growth in Lithium/Polymer Systems. *J. Electrochem. Soc.* **2003**, *150*, No. A1377.
(48) Faravelli, T.; Pinciroli, M.; Pisano, F.; Bozzano, G.; Dente, M.; Ranzi, E. Thermal degradation of polystyrene. *J. Anal. Appl. Pyrolysis* **2001**, *60*, 103−121.
(49) Han, S.; Kim, C.; Kwon, D. Thermal degradation of poly(ethyleneglycol). *Polym. Degrad. Stab.* **1995**, *47*, 203−208.
(50) Kerner, M.; Plylahan, N.; Scheers, J.; Johansson, P. Ionic liquid based lithium battery electrolytes: fundamental benefits of utilising

both TFSI and FSI anions? *Phys. Chem. Chem. Phys.* **2015**, *17*, 19569−19581.
(51) Isono, T.; Kawakami, N.; Watanabe, K.; Yoshida, K.; Otsuka, I.; Mamiya, H.; Ito, H.; Yamamoto, T.; Tajima, K.; Borsali, R.; Satoh, T. Microphase separation of carbohydrate based star block copolymers with sub 10 nm periodicity. *Polym. Chem.* **2019**, *10*, 1119−1129.
(52) Bendejacq, D.; Ponsinet, V.; Joanicot, M.; Loo, Y. L.; Register, R. A. Well Ordered Microdomain Structures in Polydisperse Poly (styrene)−Poly(acrylic acid) Diblock Copolymers from Controlled Radical Polymerization. *Macromolecules* **2002**, *35*, 6645−6649.
(53) Gilbert, J. B.; Luo, M.; Shelton, C. K.; Rubner, M. F.; Cohen, R. E.; Epps, T. H. Determination of lithium ion distributions in nanostructured block polymer electrolyte thin films by X ray photoelectron spectroscopy depth profiling. *ACS Nano* **2015**, *9*, 512−520. Published Online: Dec. 23, 2014.
(54) Sharon, D.; Bennington, P.; Webb, M. A.; Deng, C.; Pablo, J. J.; de Patel, S. N.; Nealey, P. F. Molecular Level Differences in Ionic Solvation and Transport Behavior in Ethylene Oxide Based Homopolymer and Block Copolymer Electrolytes. *J. Am. Chem. Soc.* **2021**, *143*, 3180−3190. Published Online: Feb. 22, 2021.
(55) Gartner, T. E.; Morris, M. A.; Shelton, C. K.; Dura, J. A.; Epps, T. H. Quantifying Lithium Salt and Polymer Density Distributions in Nanostructured Ion Conducting Block Polymers. *Macromolecules* **2018**, *51*, 1917−1926.
(56) Lee, D.; Jung, H. Y.; Park, M. J. Solid State Polymer Electrolytes Based on AB 3 Type Miktoarm Star Copolymers. *ACS Macro Lett.* **2018**, *7*, 1046−1050.
(57) Mott, P. H.; Dorgan, J. R.; Roland, C. M. The bulk modulus and Poisson's ratio of "incompressible" materials. *J. Sound Vibration* **2008**, *312*, 572−575.
(58) Monroe, C.; Newman, J. The Impact of Elastic Deformation on Deposition Kinetics at Lithium/Polymer Interfaces. *J. Electrochem. Soc.* **2005**, *152*, No. A396.
(59) Evans, J.; Vincent, C. A.; Bruce, P. G. Electrochemical measurement of transference numbers in polymer electrolytes. *Polymer* **1987**, *28*, 2324−2328.
(60) Pesko, D. M.; Timachova, K.; Bhattacharya, R.; Smith, M. C.; Villaluenga, I.; Newman, J.; Balsara, N. P. Negative Transference Numbers in Poly(ethylene oxide) Based Electrolytes. *J. Electrochem. Soc.* **2017**, *164*, E3569−E3575.
(61) Pożyczka, K.; Marzantowicz, M.; Dygas, J. R.; Krok, F. Ionic conductivity and lithium transference number of poly(ethylene oxide):LiTFSI system. *Electrochim. Acta* **2017**, *227*, 127−135.
(62) Atik, J.; Diddens, D.; Thienenkamp, J. H.; Brunklaus, G.; Winter, M.; Paillard, E. Cation Assisted Lithium Ion Transport for High Performance PEO based Ternary Solid Polymer Electrolytes. *Angew. Chem., Int. Ed.* **2021**, *60*, 11919−11927. Published Online: Mar. 1, 2021.
(63) Kim, G. T.; Passerini, S.; Carewska, M.; Appetecchi, G. B. Ionic Liquid Based Electrolyte Membranes for Medium High Temperature Lithium Polymer Batteries. *Membranes* **2018**, *8*, No. 41. Published Online: July 10, 2018.
(64) Chen, Z.; Steinle, D.; Nguyen, H. D.; Kim, J. K.; Mayer, A.; Shi, J.; Paillard, E.; Iojoiu, C.; Passerini, S.; Bresser, D. High energy lithium batteries based on single ion conducting polymer electrolytes and Li[Ni0.8Co0.1Mn0.1]O2 cathodes. *Nano Energy* **2020**, *77*, No. 105129.
(65) Tang, Y.; Deng, J.; Li, W.; Malyi, O. I.; Zhang, Y.; Zhou, X.; Pan, S.; Wei, J.; Cai, Y.; Chen, Z.; Chen, X. Water Soluble Sericin Protein Enabling Stable Solid Electrolyte Interphase for Fast Charging High Voltage Battery Electrode. *Adv. Mater.* **2017**, *29*, No. 1701828. Published Online: Jul. 3, 2017.
(66) Liu, B.; Zhang, J. G.; Xu, W. Advancing Lithium Metal Batteries. *Joule* **2018**, *2*, 833−845.
(67) Wan, J.; Xie, J.; Kong, X.; Liu, Z.; Liu, K.; Shi, F.; Pei, A.; Chen, H.; Chen, W.; Chen, J.; Zhang, X.; Zong, L.; Wang, J.; Chen, L. Q.; Qin, J.; Cui, Y. Ultrathin, flexible, solid polymer composite electrolyte enabled with aligned nanoporous host for lithium batteries. *Nat. Nanotechnol.* **2019**, *14*, 705−711. Published Online: May. 27, 2019.
(68) Colombo, F.; Bonizzoni, S.; Ferrara, C.; Simonutti, R.; Mauri, M.; Falco, M.; Gerbaldi, C.; Mustarelli, P.; Ruffo, R. Polymer in Ceramic Nanocomposite Solid Electrolyte for Lithium Metal Batteries Encompassing PEO Grafted TiO 2 Nanocrystals. *J. Electrochem. Soc.* **2020**, *167*, No. 70535.
(69) Wetjen, M.; Kim, G. T.; Joost, M.; Winter, M.; Passerini, S. Temperature dependence of electrochemical properties of cross linked poly(ethylene oxide)−lithium bis(trifluoromethanesulfonyl) imide−N butyl N methylpyrrolidinium bis (trifluoromethanesulfonyl)imide solid polymer electrolytes for lithium batteries. *Electrochim. Acta* **2013**, *87*, 779−787.
(70) Stolz, L.; Homann, G.; Winter, M.; Kasnatscheew, J. The Sand equation and its enormous practical relevance for solid state lithium metal batteries. *Mater. Today* **2021**, *44*, No. 9.